Chemical Engineering Journal 333 (2018) 495–504

Contents lists available at ScienceDirect

Chemical Engineering Journal

journal homepage: www.elsevier.com/locate/cej

New insights on crystal violet dye adsorption on montmorillonite: Kinetics and surface complexes studies

J.L. Marco-Brown[a], L. Guz[a], M.S. Olivelli[a], B. Schampera[b,1], R.M. Torres Sánchez[c], G. Curutchet[a], R. Candal[a,*]

[a] Instituto de Investigación e Ingeniería Ambiental, CONICET, Universidad Nacional de San Martín, Av. 25 de Mayo y Francia, 1650 General San Martín, Provincia de Buenos Aires, Argentina
[b] Institut für Bodenkunde, Leibniz Universität Hannover, Herrenhäuser Straße 2, D-30419 Hannover, Germany
[c] Centro de Tecnología en Recursos Minerales y Cerámica (CETMIC), CONICET-CCT La Plata-CIC, Camino Centenario y 506 CC (49), B1897ZCA M. B. Gonnet, Argentina

GRAPHICAL ABSTRACT

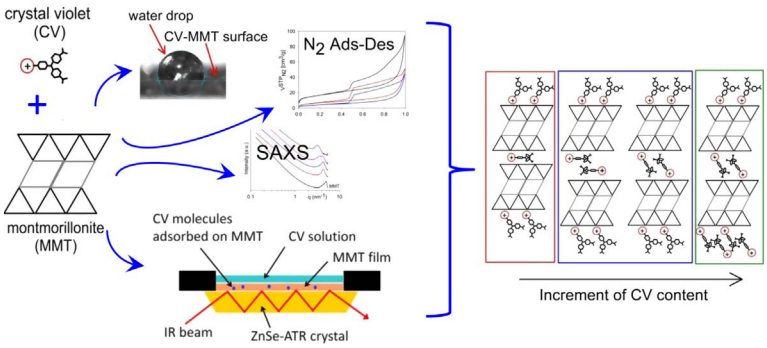

ARTICLE INFO

Keywords:
Montmorillonite
Crystal violet
Adsorption
Adsorption kinetic
In-situ FTIR
Surface complexes

ABSTRACT

Adsorption of crystal violet (CV) on montmorillonite (MMT) was investigated through kinetic analysis, microstructural characterization, surface charge and contact angle determination. Adsorption kinetic was studied in situ by attenuated total reflectance Fourier-transform infrared analysis (ATR-FTIR); MMT microstructural changes were determined by small angle X-ray scattering (SAXS) and N_2 adsorption/desorption analysis; wettability and surface charge were determined by contact angle and a particle charge detection technique, respectively.

Kinetic studies indicated that the analyzed total adsorption rate was the result of the combination of intraparticle diffusion and/or surface adsorption processes, where the contribution of each phenomenon depended on the initial concentration of CV. Obtained findings of characterization studies allowed proposing different molecular arrangements according to the concentration of adsorbed dye in water. For low CV concentration, the dye molecules entered in the MMT interlaminar space as a monolayer, with the aromatic rings parallel to the interlayer space surface. At medium CV content, the dye molecules entered the MMT interlaminar space either in a paraffin-like monomolecular arrangement with a tilt angle or in a bilayer configuration. In both cases, increment of the basal spacing, reduction of wettability, diminution of negative surface charge and the interaction of CV molecule with surface through its quaternary amine group were determined. At higher CV content, the

* Corresponding author.
E-mail addresses: joseluis.marcobrown@unsam.edu.ar (J.L. Marco-Brown), guzlucas@yahoo.com.ar (L. Guz), melisaolivelli@hotmail.com (M.S. Olivelli), birgit.schampera@dbe.de (B. Schampera), rosats@cetmic.unlp.edu.ar (R.M. Torres Sánchez), gcurut@gmail.com (G. Curutchet), rjcandal@gmail.com (R. Candal).
[1] Present address: B.S: Deutsche Gesellschaft zum Bau und Betrieb von Endlagern für Abfallstoffe mbH (DBE), Eschenstraße 55, D- 31224 Peine.

http://dx.doi.org/10.1016/j.cej.2017.09.172
Received 2 August 2017; Received in revised form 25 September 2017; Accepted 26 September 2017
Available online 28 September 2017
1385-8947/

wettability increases and surface charge shifted to positive values, indicating the presence of CV bilayer arrangements, with the positively charged region of the dye molecules facing away from the surface. Results of this work will help to develop efficient adsorbents and to achieve a deeper understanding on the fate of CV (and similar compounds) in water and sediments.

1. Introduction

Colored wastewaters from textile, plastic, paper, tannery and other industries are continuously increasing, being this phenomenon specially worrying in developing countries [1]. The dyes present in these wastewaters are typically recalcitrant and it could be rapidly spread into the environment [2,3].

The interaction between dyes and clays is particularly important in processes related with the environmental dissemination of these pollutants and also in mitigation or remediation process. Clays are present in soils, sediments and waters (as colloidal particles), playing an important role in the environmental availability and transport of different pollutants [4,5]. Moreover, clays (i.e. bentonites) and clay-composites have been extensively proposed as effective low cost absorbents for certain dyes and other organic and inorganic pollutants [6–12]. Montmorillonite clay (MMT) (belonging to the smectite group) has been broadly studied as an adsorbent for synthetic dyes [13–16]. However, given the enormous complexity of adsorption processes in the environment, the use of simple pollutant-clay models acquires great importance and interest to thoroughly understand the basic interactions between adsorbate and sorbate.

MMT has an aluminum-silicate layered structure with a net negative charge generated by isomorphic substitutions. The intrinsic negative charge is compensated with inorganic cations (typically Na^+ or Ca^{2+} ions). The high cationic exchange capacity, high specific surface area and intrinsic negative charge make MMT a promising adsorbent for cationic synthetic dyes [16].

Triarylmethane dyes (TAM) are recalcitrant dyes that have been used as antimicrobial and antifungal agents [17,18]. These compounds have a net positive charge, being crystal violet (CV) a good representative for cationic dyes. CV also presents the phenomenon known as metachromicity, where a shift in the maximum absorption wavelength according to dye concentration is observed, and it was demonstrated that at high concentrations it could form dimmers both in solution as well as adsorbed on clay minerals [19–24].

Adsorption of CV on MMT was previously studied by other authors [15,19–23,25–29]; more specifically, metachromicity was used in early studies to explore the different possibilities of CV adsorption on MMT [19–23,26]. Recent studies remark the importance of the adsorption of organic molecules (in particular CV molecules) at the surface and/or in the interlaminar space of MMT, modifying the wettability of the system and its interaction with other pollutants [16,28]. These may lead to new relevant technological applications of the obtained MMT-CV complexes, e.g., as adsorbents for hydrophobic organic contaminants [28,29] or as precursors for synthesizing graphene-like carbon nanomaterials [30,31].

Few works report studies on kinetics, thermodynamic and structural characteristics of CV adsorption on MMT [27,32,33]. Nevertheless, an extensive analysis of CV adsorption on MMT is required in order to understand the overall adsorption process mechanism. This knowledge is necessary to better understand the localization and arrangement of CV at MMT and its effect on surface properties, which determine the interaction of the sorbent/sorbate system with other pollutants and, in general, the surrounded environment [16]. Recently, it was proposed the use of Attenuated Total Reflectance Fourier Transform Infrared (ATR-FTIR) spectroscopy as a novel methodology for in-situ adsorption kinetic studies of organic molecules on montmorillonite [5]. This technique may provide further insight in the adsorption kinetic and mechanism of CV adsorption on MMT improving the present understanding on the adsorption of organic cations on montmorillonite.

The aim of this work is to understand the CV adsorption mechanism on MMT by in-situ kinetic study using ATR-FTIR method, as well as studying the microstructure and surface characteristic of CV-MMT adsorption complexes. Small Angle X-ray Scattering (SAXS) and N_2 adsorption analysis were used to determine changes in the micro and nanostructure. Wettability and surface charge were determined by contact angle and charge titration measurements, respectively. This is the first time, to the best of our knowledge, that this combination of advanced and conventional techniques was used together on dye-montmorillonite complexes in order to determine the dye adsorption mechanism in a wide range of concentrations. The results of this study will help in the design of better adsorbents for cationic organic contaminants, the development of more efficient sorption or pollutants mitigation treatments and in selecting optimum operating conditions for full-scale batch process.

2. Experimental details

2.1. Materials

Smectite collected from Lago Pellegrini deposit (Rio Negro, North Patagonia, Argentine) was provided by Castiglioni Pes y Cia. Cationic exchange capacity (CEC), determined by the Cu-triethylenetetramine method [34], was 0.825 mmol/g clay. Isoelectric point (IEP), obtained by the determination of the diffusion potential as described elsewhere [35], was 2.7. The mineralogy and chemical analysis of this smectite were determined in a previous work [36]. XRD and chemical analysis indicated that contained mostly Na-montmorillonite (> 99%) with quartz and feldspars as minor phases. The structural formula determined from the chemical composition (%) following the procedure proposed by Siguin et al. [37] was $[(Si_{3.89}Al_{0.11})(Al_{1.43}Fe_{0.28}Mg_{0.30})O_{10}(OH)_2]Na^+_{0.41}$ (more details in Ref. [36,38]). Crystal violet (CV) dye (Analytical grade, C.I. 42555, chemical formula = $C_{25}H_{30}N_3Cl$, Mol. wt. = 407.99 g/mol, λ_{max} 590 nm) was purchased from Biopack (Argentina).

2.2. Adsorption kinetics

Attenuated total reflectance Fourier transform infrared spectra (ATR-FTIR) were performed with a Tensor 27, Bruker spectrometer (200 scans, resolution 4 cm^{-1}) on a ZnSe-ATR crystal unit (area = 10 mm × 72 mm) with an incident angle of 45° and 11 reflections. A thin colloidal film of MMT was deposited onto an ATR crystal by placing 0.5 mL of a MMT colloidal dispersion (0.31 gL^{-1}) and evaporating to dryness at room temperature as indicated in a previous work [5]. The MMT film was rinsed with small aliquots of water to eliminate loosely deposited particles.

A volume of 1.4 mL of a 1×10^{-2} $molL^{-1}$ KCl was placed on the MMT film and MMT spectra were recorded. Then, the KCl solution was withdrawn and a volume of 1.4 mL of CV fresh solution at constant ionic strength of 1×10^{-2} $molL^{-1}$ KCl, was placed on the MMT film. The initial concentration of CV in solution, $[CV]_0$, was varied from 0.12 to 1.23 $mmolL^{-1}$, and the pH of all the solutions was adjusted to 7.0. This range covers the concentrations typically used to prepare CV-MMT complexes and allows the comparison between kinetic adsorption and structure/surface CV-MMT complexes experiments. ATR-FTIR spectra were recorded as a function of time at room temperature until no further changes were detected. This indicated that the film was saturated

with the adsorbate. Temporal changes measured as the absorbance (A_t) were quantified by monitoring the changing absorbance of each selected vibration frequency. A scheme of the experimental setup for the study of CV adsorption kinetics on MMT films is showed in Fig. S1, Supporting Information.

Typical CV vibration frequencies centered at 1588, 1367 and 1184 cm^{-1}, due to C=C, N-Ph and N-CH_3 stretching respectively (details will be given later), were monitored to determine CV kinetic adsorption for each $[CV]_0$. Experiments were performed by duplicated. The FTIR spectrum of the MMT film (in the presence of a solution containing 1×10^{-2} mol L^{-1} KCl) was considered as a background and it was subtracted from the spectra obtained for all in situ adsorption experiments to monitor exclusively the change by addition of CV. Kinetic models were tested for simulation of the experimental data, being obtained six sets of a model parameters for each $[CV]_0$, which were averaged.

The spectrum of each CV solution was previously recorded in the absence of the MMT film. Furthermore, the FTIR spectra of the CV solutions were compared to FTIR spectra of CV adsorbed on MMT films at equilibrium time (CV@MMTfilm) in order to determine CV groups involved in the adsorption process.

2.3. MMTCV samples preparation

Solid samples containing different concentration of crystal violet adsorbed on montmorillonite (MMTCV) were prepared by adsorption of CV on MMT dispersions (1gr L^{-1}) as indicated in a previous work [15] using a CV initial concentration $[CV]_0$ ranging from 0.06 to 1.96 mmol L^{-1} at constant ionic strength of 1×10^{-2} mol dm^{-3} KCl. The dispersions were shaken and equilibrated for 12 h at room temperature. Subsequently, the dispersions were centrifuged 15 min at 13,500 rpm and the pellet obtained was separated from the supernatant solution. The solids were washed with deionized water two times, centrifuged, dried at 60 °C overnight and stored in desiccators over silica gel, at room temperature, for further analysis and labeled, e.g., as MMTCV0.12 for a sample prepared from a CV solution with CV initial concentration $[CV]_0 = 0.12$ mmol L^{-1}.

2.4. Interlaminar space determination by SAXS/WAXS

Samples of pure MMT and MMTCV samples were characterized by Small Angle X-ray Scattering (SAXS) and Wide Angle X-ray Scattering (WAXS) to determine changes in the interlaminar space. Data were obtained at the D01A SAXS line workstation of the Brazilian Synchrotron Light Source (LNLS), Campinas, Brazil, using a wavelength of 0.155 nm and a sample to detector distance of 491.334 mm. The range of q detected allowed spanning $0.25 \leq q \leq 5.9$ nm of range. All measurements were made at room temperature and registered in a 2D-CCD detector (MAR-USA 165 mm).

2.5. N_2 adsorption-desorption isotherms

Nitrogen adsorption-desorption on MMT and MMTCV samples isotherms were recorded at 77 K using the NOVA 4000e Surface Area & Pore Size Analyzer from Quantachrome Instruments. The specific surface area was calculated using the BET method. Total pore volume (V_{TP}) was calculated by Gurvitch method. Diameter pore size for a slit pore (W_P) calculated as $W_P = 2 \cdot V_{TP}/S_{BET}$. All samples were degassed at 120 °C by the FloVac Degasser (Quantachrome Instruments) for at least 12 h prior to measurement.

2.6. Surface charge and wettability

The surface charge (SC) of MMT and MMTCV samples were quantified as indicated in a previous work [39,40] by generating a streaming potential and titration of charge-compensating polyelectrolytes using the cell of a particle charge detector (PCD 03, Mütek, Germany). For negative and positive SC, the cationic polyelectrolyte poly-DADMAC (poly-diallyldimethylammonium chloride) and the anionic polyelectrolyte PES-Na (sodium polyethylene sulfonate) were used, resp. The particle charge detection (PCD) technique is a well-established method for studying SC properties of modified clays [39–41]. For each titration, 10 mg of sample was suspended in 10 mL of deionized water. After dispersion, the suspension was transferred into the titration cell. Each measurement was performed at least three times.

Contact angle (CA) of MMT and MMTCV samples were measured to determine their wettability. The sessile drop method was applied using a charge-coupled device (CCD) equipped contact angle microscope (OCA 15, DataPhysics, Filderstadt, Germany) allowing the evaluation of CA at any time after droplet placing. A drop of deionized water (V = 3 µl) was placed on the sample, which was sprinkled and gently pressed to establish a firm connection to a double-sided adhesive tape on a microscopic glass slide. The initial CA (30 ms after placement of the drop and ending of mechanical perturbations) was analyzed by automated drop shape analysis (ellipsoidal fit) and fitting tangents to both sides, using the software SCA20 (DataPhysics, Filderstadt, Germany) [42–44]. Each measurement was performed at least six times.

3. Results and discussion

3.1. FTIR analysis

FTIR spectra of different CV solutions in 1×10^{-2} mol L^{-1} KCl were determined and compared with FTIR spectra of CV adsorbed on MMT films at equilibrium time (CV@MMTfilm) (Fig. 1). The peaks between 1590 and 1480 cm^{-1} are typically assigned to C=C stretching vibration of aromatic rings. The band centered at 1367 cm^{-1} had been attributed to N-phenyl stretching vibration and the doublet with peaks at 1176 and 1192 cm^{-1} to N-CH_3 stretching vibration [28,45,46]. The absorbance of FTIR vibration showed higher values as the initial concentration of CV increased, indicating that at higher initial concentrations higher amount of CV was adsorbed on MMT (Table S1, Supporting

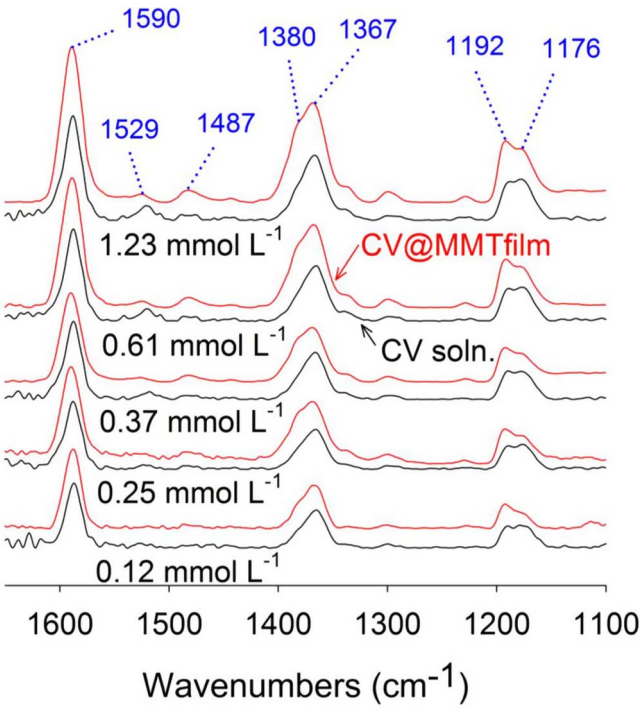

Fig. 1. FTIR spectra of CV solutions and CV adsorbed on MMT films at equilibrium time (CV@MMTfilm). $[CV]_0$ are indicated.

Information). The appearance of a shoulder at 1380 cm^{-1} and the increment of the intensity of the peak at 1192 cm^{-1} observed in CV@MMT film respect to the CV solution for the whole CV initial concentrations studied, could be attributed to the interaction of CV with MMT surface. A similar shift was observed before [28] and was attributed to the strong interaction between CV and MMT.

The effect of pH on CV adsorption was studied in batch systems for a $[CV]_0$ of 1.23 mM in MMT dispersions of 1 gL^{-1} (Figure S2, Supporting Information). Results evidenced that at higher pH values, the CV adsorption on MMT was increased. Similar results were reported for CV adsorption on MMT and other adsorbents [27,47,48]. Zeta potential studies performed with MMT showed that the surface was negatively charged throughout the whole pH-range, with negative charges increasing as the pH increased [15]. The experimental evidence indicated that the interaction of CV with the clay mineral surface was typically electrostatic (i.e. the adsorption of cations is favored by an increment of pH due to the augment of MMT negative surface charge). This behavior agrees with the coordination of the CV molecule with surface sites through the interaction of its quaternary amine by means of the formation of an outer-sphere complex. An interaction of CV with clay surface through its quaternary amine is in accordance with shifts of peaks corresponding to N-phenyl and N-CH_3 stretching vibrations indicated in the previous paragraph.

3.2. Adsorption kinetics

Adsorption of CV onto MMT films from solutions containing different $[CV]_0$ in 1×10^{-2} $molL^{-1}$ KCl was determined by in situ FTIR. Fig. 2 shows a typical FTIR spectrum of CV adsorbed on MMT film from a CV solution of $[CV]_0 = 0.12$ $mmolL^{-1}$.

Peaks centered at 1588, 1367 and 1184 cm^{-1} were used to follow the kinetic adsorption of CV onto MMT. The area of the bands varied monotonously over time as CV was being adsorbed onto MMT clay.

By applying Beer-Lambert law, the band area at a given time (A_t) and the band area at the adsorption equilibrium (A_e), are directly related to the degree of surface coverage (θ_t) and to the degree of surface coverage at the adsorption equilibrium (θ_e), resp. [5,49–51]. Additionally, the ratio A_t/A_e is equivalent to the ratio θ_t/θ_e. Fig. 3 shows θ_t normalized by θ_e (θ_t/θ_e) versus evolution over time for the band centered at 1367 cm^{-1}. Similar behavior was obtained for the evolution of θ_t/θ_e over time using bands centered at 1588 and 1184 cm^{-1} at all $[CV]_0$ (Figure S3, Supporting Information, shows the evolution over time of the bands centered at 1588 and 1184 cm^{-1}). The evolution over time of θ_t/θ_e was found to be very reproducible, although the adsorption capacity showed fairly large variations for individual experiments. This latter feature has been attributed to random changes in the fraction of the film that is actually available for adsorption [52]. Equilibrium conditions were reached after 20 and 80 min for the higher and lower CV initial concentration, resp.

3.3. Kinetic models

Several kinetic models including Lagergren pseudo-first-order (PFO), pseudo-second-order (PSO), intra-particle diffusion model (IDM) [5,53,54] were tested for simulation of the experimental data. Table 1 shows the parameters obtained by fitting the experimental data to the different models.

The PFO equation [55], widely used for biosorption, is based on a Lagergren pseudo-first-order rate expression:

$$\ln(\theta_e - \theta_t) = \ln\theta_e - k_1 t \quad (1)$$

where k_1 is the pseudo-first-order sorption rate constant, θ_e and θ_t are the surface coverage at equilibrium and at any time t, resp. As mentioned before, θ_e and θ_t were measured as the area beneath the bands centered at 1588, 1367 and 1184 cm^{-1}. It is necessary to relate θ_t to θ_e (θ_t/θ_e) in these kind of systems in order to made them independent of the thickness of the MMT film allowing the results to be comparable between experiments [5,52]. The overall rate constant, k_1, (Table 1) was calculated from the slope by plotting $\ln(1 - \theta_t/\theta_e)$ versus t (Fig. S4, Supporting Information). The coefficients of determination (R^2) obtained using the Lagergren model for the evaluated bands were lower than 0.96.

Pseudo-second-order (PSO) equation assumes that the adsorption rate is proportional to the square of the number of unoccupied surface sites [53]. Moreover, the number of occupied sites is proportional to the adsorbate concentration. PSO equation is defined by Eq. (2) and the integrated form is given in Eq. (3).

$$\frac{d\theta_t}{dt} = k_2(\theta_e - \theta_t)^2 \quad (2)$$

$$\frac{t}{\theta_t} = \frac{1}{k_2\theta_e^2} + \frac{t}{\theta_e} \quad (3)$$

θ_e and θ_t are the surface coverage at equilibrium and at a determined time t, respectively; and k_2 is the sorption rate constant. The kinetics parameters k_2 and θ_e are typically obtained from the slope and intercept of a t/θ_t vs t plot. However, to normalize the systems and to induce an independence to the thickness of the MMT film, $t*\theta_e/\theta_t$ versus time plots were performed. Fig. 4 shows the plot of $t*\theta_e/\theta_t$ versus time (t) for the band centered at 1367 cm^{-1} at the CV initial concentrations. Fig. S5, Supporting Information, shows plots of $t*\theta_e/\theta_t$ versus time (t) for bands centered at 1588 and 1184 cm^{-1}. Linear plots were obtained in all the cases. However, as the CV initial concentration decreases, bigger deviations from the PSO model were observed. As shown in Table 1, the slope and the intercept differ from the expected values (1 and 0, resp.). An intercept value different from zero or a deviation from linearity at initial times had been attributed to a greater contribution of a diffusional process [53,56]. In our study, this phenomenon was likely caused by the contribution of a diffusional process at low initial CV concentration as will be addressed below.

Taking into account the possible existence of a diffusional process contributing to the global adsorption rate, the intraparticle diffusion model (IDM) was investigated to analyse the adsorption kinetic data.

The IDM is applicable when the rate-determining step is the mass transfer of the adsorbate to the solid surface sites. Several authors use Eq. (4) based on the model of Weber-Morris [57] in order to adjust experimental data to the IDM:

$$\theta_t = k_{id}\sqrt{t} + C \quad (4)$$

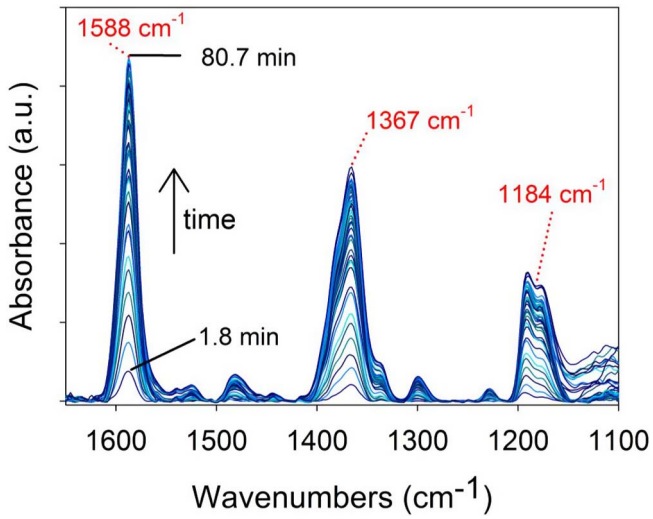

Fig. 2. Evolution of peaks at 1588, 1367 and 1184 cm^{-1} over time in a typical CV adsorption onto MMT film. Kinetic experiment using $[CV]_0 = 0.12$ $mmolL^{-1}$. Time interval is indicated in the figure.

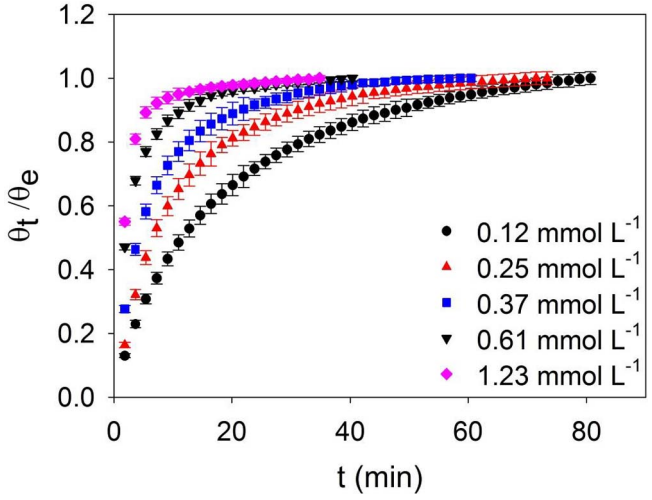

Fig. 3. Temporal evolution of θ_t normalized by θ_e ($\theta t/\theta e$) for the band centred at 1367 cm^{-1} (N-phenyl stretching vibration) for CV adsorption onto MMT. $[CV]_0$ are indicated.

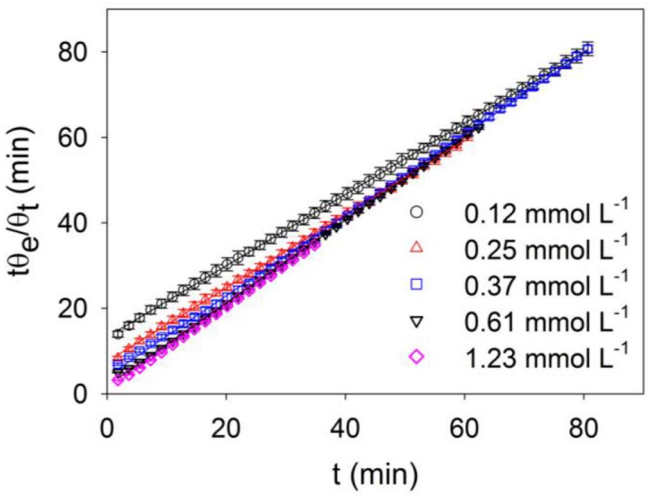

Fig. 4. $t^*\theta_e/\theta_t$ versus time (t) linear plots for the band centered at 1367 cm^{-1}. The solid line was obtained from Eq. (2) (PSO). $[CV]_0$ are indicated.

where k_{id} is the intraparticle diffusion constant and C is the intercept of the linear plots. If the intraparticle diffusion is the only rate-limiting step, the linear plot of θ_t versus $t^{1/2}$ should pass through the origin. But, if the intercept C of plots is not equal to zero, the intraparticle diffusion is not the solely rate-determining step.

Plots of θ_t/θ_e at 1367 cm^{-1} versus $t^{1/2}$ for CV adsorption on MMT film at different CV initial concentrations are shown in Fig. 5. Fig. S6, Supporting Information, shows plots of θ_t/θ_e versus $t^{1/2}$ for bands centered at 1588 and 1184 cm^{-1}. The diffusion kinetic plots exhibited the three-stage linearity which indicated that the adsorption process occurs in two or more steps [58,59]. The first section of the plot (corresponding to initial times) was attributed to high adsorption rate on the external surface of the adsorbent, which presented sufficient available adsorption sites. Afterwards, while external surface sites reached saturation, the CV molecule came across much larger hindrance because of its transference through farther and deeper inner pores of MMT where the intraparticle diffusion was the rate-controlling step. The ratio between intra-particle diffusion rate k_{id} and θ_e ($k_{id}\theta_e^{-1}$) and $C\theta_e^{-1}$ values were obtained from the slope and intercept from the linear regression of the second section (intermediate times) of the plot, resp., [59,60] and are presented in Table 1. In addition, the plots did not pass through the origin, which indicated that diffusion through the pores was not the limiting factor [59,61]. Finally, the third section was the final equilibrium stage, where the intraparticle diffusion started to slow down due to the low remnant CV concentration in the solution [59].

The increase of adsorbate concentration resulted in an increase of the concentration gradient between the porous and the solution bulk, which increased the diffusion rate of the adsorbate, k_{id} [59,62]. The

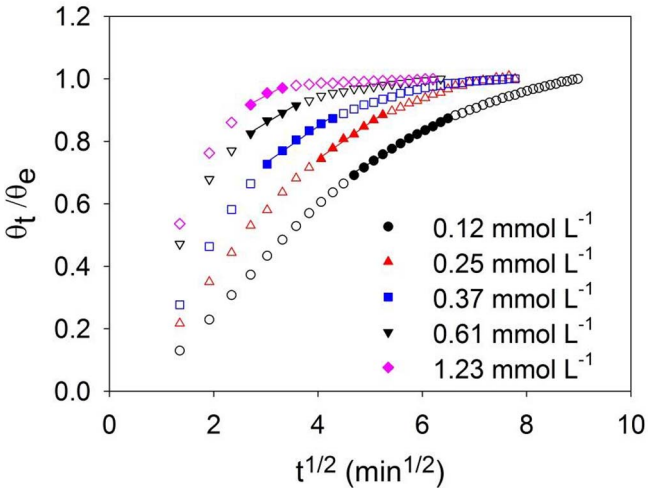

Fig. 5. Plots of θ_t/θ_e versus $t^{1/2}$ for the band centered at 1367 cm^{-1}. Full filled dots are related to the intraparticle diffusion stage and its linear regression was used to determine $k_{id}\theta_e^{-1}$ and C values (Eq. (4)). Empty dots at initial times are related to high adsorption rate on the external surface. Empty dots at final times correspond to the final equilibrium stage. $[CV]_0$ are indicated.

calculated intraparticle diffusion coefficient, k_{id}, related to θ_e ($k_{id}\theta_e^{-1}$) values at different initial dye concentrations are shown in Table 1. Results indicated that an increase of CV initial concentration caused no change in the $k_{id}\theta_e^{-1}$ value; nevertheless, θ_e value increased with $[CV]_0$ [15], consequently, the k_{id} value should increase with $[CV]_0$. On the other hand, the C value (Eq. (4)) reflected the boundary layer effect ([53] and references therein). The larger the value of the intercept of

Table 1
Pseudo-first order (PFO), Pseudo-second order (PSO) and Intraparticle diffusion model (IDM) parameters of CV adsorption on MMT kinetics for $[CV]_0$ 0.12; 0.25; 0.37; 0.61 and 1.23 mmol L^{-1} obtained by adjusting experimental data by Eqs. 1, 3 and 5, respectively.

	Kinetic Model							
	Pseudo-first order		Pseudo-second order			Intraparticle diffusion		
$[CV]_0$ (mmol L^{-1})	k_1 (min^{-1})	R^2	$\theta_e k_2$ (min^{-1})	m	R^2	$k_{id}\theta_e^{-1}$ ($min^{-1/2}$)	$C\theta_e^{-1}$	R^2
0.12	−0.06 ± 0.01	0.9374	0.075 ± 0.004	0.84 ± 0.02	0.9999	0.10 ± 0.01	0.24 ± 0.02	0.9944
0.25	−0.08 ± 0.01	0.9598	0.14 ± 0.01	0.89 ± 0.02	0.9994	0.12 ± 0.01	0.28 ± 0.02	0.9927
0.37	−0.08 ± 0.02	0.9611	0.24 ± 0.02	0.92 ± 0.02	0.9996	0.12 ± 0.01	0.38 ± 0.02	0.9878
0.61	−0.10 ± 0.02	0.9598	0.52 ± 0.08	0.96 ± 0.02	0.9998	0.10 ± 0.01	0.55 ± 0.02	0.9876
1.23	−0.14 ± 0.01	0.9075	1.0 ± 0.1	0.97 ± 0.02	0.9997	0.09 ± 0.01	0.68 ± 0.02	0.9608

the plot is, the greater is the contribution of the surface sorption in the rate-limiting step. The increase of k_{id} and $C\theta_e^{-1}$ with $[CV]_0$ indicated that the diffusion process was less important in samples with high CV initial concentration, and the surface adsorption became the rate-limiting step. Hence, the three-stage linearity of intraparticle diffusion plots confirmed the presence of both surface adsorption and intraparticle diffusion [59] as was proposed by PSO modelling. Thus, the adsorption process might present a complex nature, involving both surface adsorption and intraparticle diffusion [58,59]. An explanation of the relation between the MMTCV surface complexes formation and the CV adsorption kinetics will be discussed later.

3.4. WAXS/SAXS analysis

WAXS and SAXS patterns for MMT and MMTCV samples are shown in Fig. 6. Shifts of the signal corresponding to basal spacing towards higher values of scattering vector *q*, with respect to raw MMT, can be observed in all MMTCV samples, indicating the incorporation of CV molecule into the interlayer spaces of MMT. Basal spacing was calculated with equation 5:

$$q = (4\pi \text{sen}\theta)/\lambda \quad (5)$$

where 2θ is the angle between the incident X-ray beam and the detector measuring the scattered intensity, and λ is the wavelength of the X-rays.

A basal spacing of 1.25 nm was obtained for raw MMT, which agree with values previously determined by X-ray diffraction [4]. For low CV content (MMTCV0.12 and MMTCV0.25 samples), an increment of basal spacing to 1.45 nm was obtained. A basal spacing of 1.94 nm was found for a high CV content (MMTCV0.61 to MMTCV1.96). For MMTCV0.37, it was observed the coexistence of two basal spacing (1.45 and 1.94 nm) in the same sample. The molecular modeling of the CV molecule was done using HyperChem 8.0.5 software [63] to determine its dimensions. After applying geometry optimization, the molecule dimensions were approximately estimated and a planar molecule was obtained (0.44 nm in width and 1.3 nm in length). Once the dimensions were calculated the orientation of the CV incoming molecule in the interlayer space can be estimated. This kind of modeling is commonly used to determine molecule dimensions and its entry in the interlayer space of layered systems [4,64]. Taking into account its molecular dimensions, the CV molecules may be accommodated into the clay interlayer space in different arrangements. The first one (for a basal spacing of 1.45 nm) corresponds to a CV planar arrangement with respect to the interlayer space surface (Fig. 7A). This result agrees with data reported by Zhu R. et al. [28]. For a basal spacing of 1.94 nm, two different arrangements are proposed: (i) a CV bilayer configuration, parallel to the interlayer space surface and (ii) a paraffin-like monomolecular arrangements ([64,65] and references therein) with tilt angles (α) of 48°, occurring an interaction of CV molecule with mineral clay surface through its quaternary amine (Fig. 7B and Fig. 7C). CV planar arrangement in the interlayer space of montmorillonite and a π interaction occurring between the dye cation and the alumino-silicate layer had been reported before [21]. In the bilayer and paraffin-like monomolecular arrangements, a $\pi \rightarrow \pi*$ interaction may occurs between CV molecules ([19] and references therein). Moreover, an interaction of CV with clay surface through its quaternary amine, as was indicated by FTIR analysis (Fig. 1), may occurs in paraffin-like monomolecular arrangements.

3.5. N_2 adsorption/desorption

In order to determine the textural properties and to obtain a better understanding of the bonding process between CV and MMT, N_2 adsorption/desorption isotherms were performed on MMT and CVMMT samples. Specific surface area (S_{BET}), total pore volume (V_{TP}) and average pore size (W_P), determined by N_2 adsorption are listed in Table 2 for MMT and MMTCV samples. Fig. 8A and B show a detail of N_2 adsorption/desorption isotherms for MMT and MMTCV (complete isotherms are presented Fig. S7, Supporting Information) The isotherms could be termed Type IIb with a H3 loop and no indication of a plateau at high P/P_0 was observed [66]. Therefore no indication of the completion of mesopore filling was evidenced. Such isotherm shape indicated that the material contains mesopores, which were responsible for the hysteresis, and macropores, which results in the absence of the plateau at high P/P_0 values. These kinds of isotherms are given by either slit-shaped pores or, as in the present case, assemblages of platy particles [66].

The decrease of S_{BET} and V_{TP} with CV content (from MMT to MMTCV0.18) was assigned to the diminution of micro-, meso- and macropores (as seen in Fig. 8A) due to: the CV arrangement in the interlayer space of MMT, occupancy of the dye in the interparticle pores, and on the external surface [65] (Fig. 7A). An increase of the S_{BET} area and the V_{TP} was observed from samples containing over 0.25 mmol L^{-1} of CV as initial concentration (as seen in Fig. 8B). This effect was the result of, on one hand, the paraffin-like monomolecular arrangements with tilt angles of the CV molecule in the MMT interlayer space, as stated by SAXS/WAX analysis, resulting in an increment of the MMT basal spacing (Fig. 7B). On the other hand, the adsorption of CV on the external surface of MMT resulted in an enlargement of the meso and macropores (Fig. 8 and S7). An increase in the W_P was observed from MMT to MMTCV0.25 samples due to an increase of the space between platy particles of the MMT. From that point, the value of W_P remained almost constant due to a change in the arrangement of the CV molecule inside the basal spacing, resulting in a new setting as a paraffin-like monomolecular arrangement (Fig. 7B). This new type of arrangement allowed the entrance of a higher amount of CV molecules into the interlayer space according to SAXS/WASX and to contact angle and surface charge studies; as will be further discussed below in the text. Thus, for samples with a higher amount of CV content (from MMTCV0.61 samples onwards) an increase of W_P values occurred due to the formation of a bilayer of CV at the external surface (Fig. 7C) causing an increment of the space between platy particles as will be explained later.

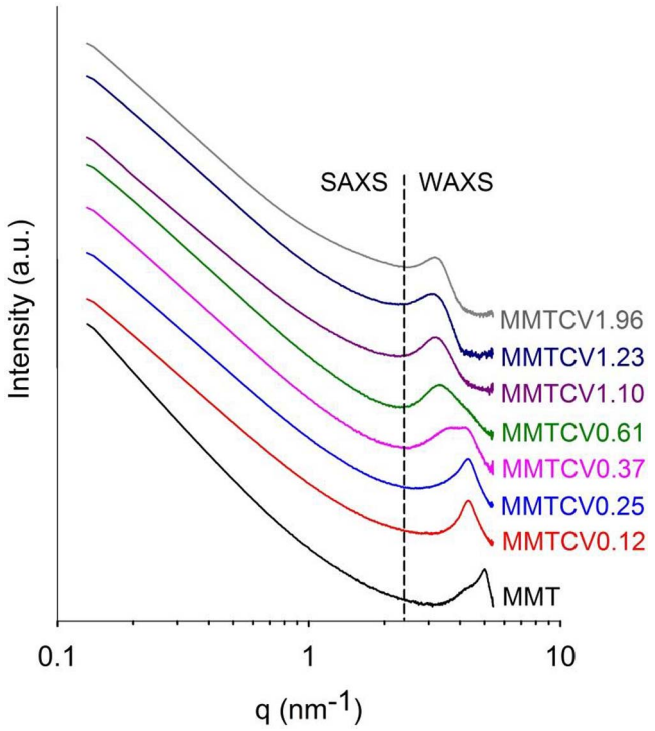

Fig. 6. Log-log SAXS/WAXS patterns for raw MMT and MMTCV samples. Plots have been displaced vertically for a better understanding.

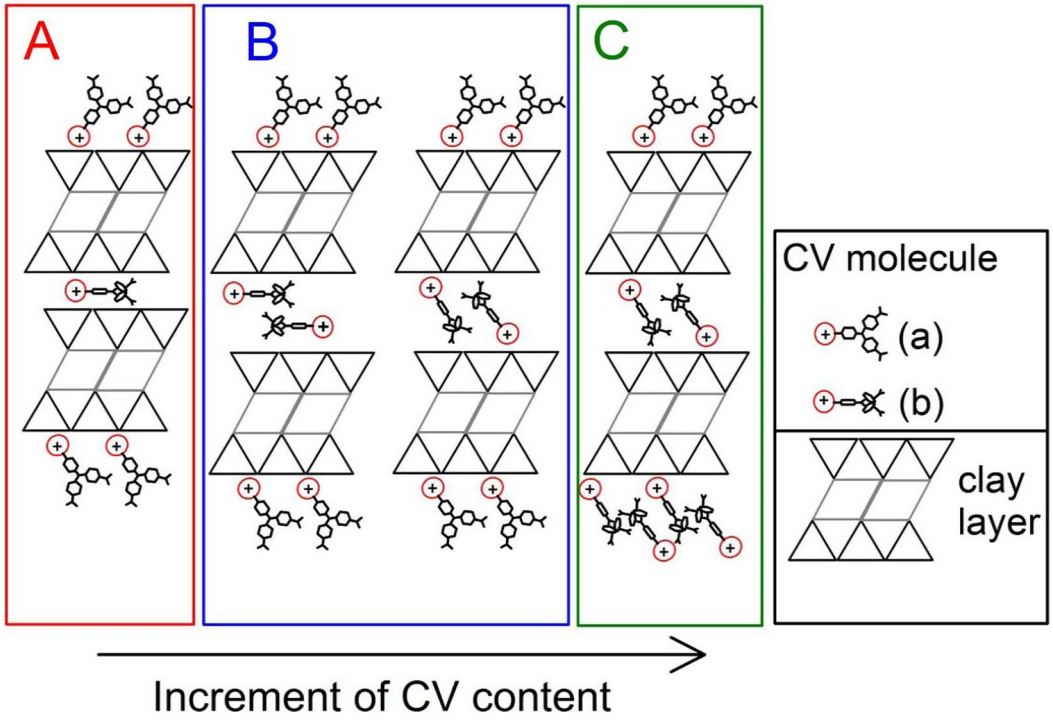

Fig. 7. Schematic interlayer and external CV complexes on MMT. (A) Low CV content, (B) medium CV content and (C) high CV content. CV interacts with MMT surface through its quaternary amine in external surface. The arrangement (a) represents molecules of CV attached to the MMT surface, with random orientation. CV planar arrangement (b) permits its π interaction with alumino-silicate layer at the interlayer space (A) and π → π* interaction between CV molecules at the interlayer space and external surface (B and C).

Table 2
Textural properties of MMT and MMTCV samples.

Sample	S_{BET} ($m^2 g^{-1}$)[a]	V_{TP} ($cm^3 g^{-1}$)[b]	W_P (nm)[c]
MMT	59 ± 4	0.078	2.7
MMTCV0.12	24 ± 1	0.045	3.6
MMTCV0.18	15 ± 1	0.036	4.8
MMTCV0.25	18 ± 1	0.047	5.1
MMTCV0.37	22 ± 1	0.058	5.2
MMTCV0.61	33 ± 2	0.090	5.5
MMTCV1.23	43 ± 1	0.138	6.5

[a]Surface area (S_{BET}) calculated by BET method. [b]Total pore volume (V_{TP}) calculated by Gurvitch method. [c]Average diameter pore size for a slit pore (W_P) calculated as $W_P = 2 \cdot V_{TP}/S_{BET}$.

3.6. Surface charge and wettability

For a detailed insight on the adsorption process, surface charge (SC) and wettability were related to the CV content in MMTCV complexes and results are illustrated in Fig. 9 and Table S2, Supporting Information. An increase of SC and decrease of wettability occurred when the CV was adsorbed on MMT at low CV content (from MMTCV0.06 to MMTCV0.18 samples; see square area *a* in Fig. 9). The entrance of the CV molecule and the CV adsorption on the external surface of MMT produced a decrease of its negative SC due to the positive charge of the CV molecule. The occupancy of external surface sites by CV molecules occurred by an interaction of the CV molecule through its quaternary amine group, facing away of the surface the non-charged CV triarylmethane group, which made possible an increment in the hydrophobicity of MMTCV complexes. This CV arrangement is well illustrated in Fig. 7A. Both, SC and wettability remained constant for samples from MMTCV0.25 to MMTCV0.61 (see square area *b* in Fig. 9) due to the entrance of CV molecules into the interlayer space in a paraffin-like monomolecular with tilt angle or in a CV bilayer configuration, parallel to the interlayer space surface, arrangements as explained before. In this kind of molecules setting, external surface sites were fully occupied and CV adsorption occurred in the interlayer space (Fig. 7B). An increment of SC and wettability was observed in samples with high CV content (from MMTCV0.74 to MMTCV0.98; see square area *c* in Fig. 9). SC became positive and wettability increased due to a bilayer CV arrangement on the surface as it is shown schematically in Fig. 7C. A similar behavior was reported before for adsorption of hexadecylpyridinium chloride on montmorillonite [39].

The previous results indicated that for low CV content, the dye entered into the MMT interlayer space in a planar configuration and it was adsorbed to the external surface forming a monolayer interacting through its quaternary amine group. When the CV content was increased, the external surface was fully occupied and the CV molecules entered in the interlayer space in a paraffin-like monomolecular with tilt angle or in a CV bilayer configuration arrangements. For high CV content samples, the dye molecule formed a bilayer on the external surface of MMT. At the external surface it might occur a π → π* interaction between CV molecules as stated before. As expected, the surface charge and wettability of these complexes depended on the CV content.

4. Conclusions

The combination of kinetic models with structural characterization, surface charge and contact angle analysis, leaded to a complete description of the sorption process of CV on MMT in a wide range of CV initial concentrations. The different mechanism that control the adsorption kinetics can be related with changes in the distribution of CV at MMT surface and interlayer space. At low $[CV]_0$, CV molecules enter into the MMT interlayer space with a planar arrangement, being simultaneously adsorbed at MMT external surface, through the formation of outer sphere complexes via electrostatic interactions between the negative MMT sites and the CV quaternary amine group, with the triarylmethane group facing away from the surface. Under these conditions, the surface adsorption is fast and diffusional process governs the adsorption kinetics.

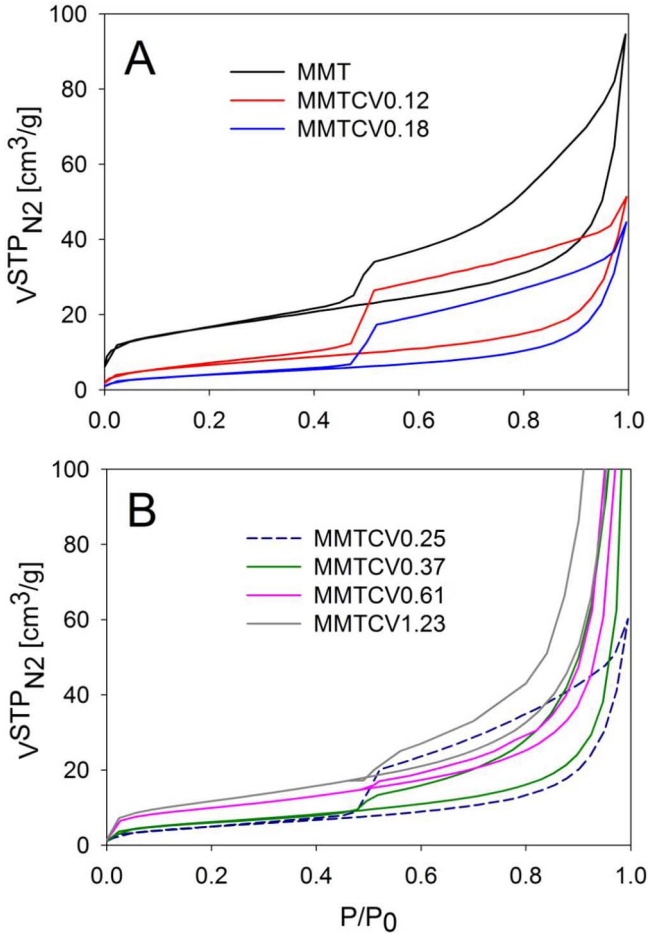

Fig. 8. Nitrogen adsorption/desorption isotherms for: (A) raw MMT and low $[CV]_0$ (0.12 and 0.18 mmolL^{-1}); (B) medium $[CV]_0$ (0.25 and 0.37 mmolL^{-1}) and high $[CV]_0$ (0.61 and 1.23 mmolL^{-1}). A full-scale figure can be find in Fig. S7.

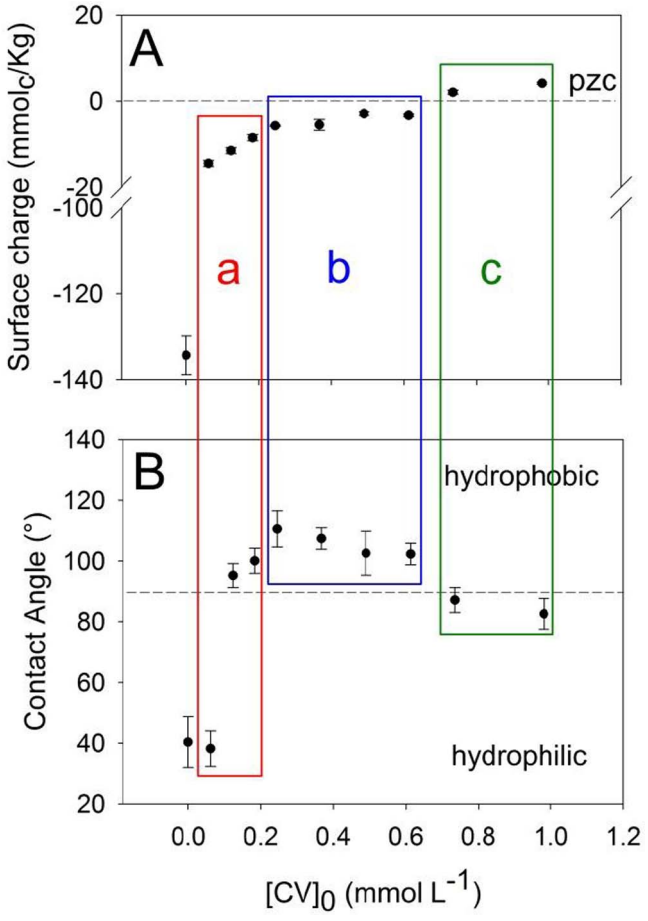

Fig. 9. (A) Surface charge and (B) contact angle of raw MMT and MMTCV samples in function of the $[CV]_0$.

At medium and high $[CV]_0$, the CV molecules located in the interlayer space adopt a paraffin-like monomolecular arrangement with tilt angles (α) of 48° or a CV bilayer configuration, parallel to the interlayer space surface. The CV molecules approaching the surface must be accommodated in the bilayer, which required its rearrangement. Under this situation, the diffusional process was negligible and the surface sorption rate governed the kinetics. At medium $[CV]_0$, the CV molecules were absorbed at the external surface of MMT with the triarylmethane group facing away from the surface occupying all available external surface sites of MMT. At high $[CV]_0$, the adsorbed molecules form a bilayer with half of the CV molecules exposing the quaternary ammonium to the solution.

Depending on CV coverage, changes in SC and wettability of the CVMMT systems were observed. At low coverage, the surface showed high wettability and negative SC, at intermediate coverage wettability was low and the SC close to zero, while at high coverage the surface wettability increased and SC was slightly positive. These results indicate that the interaction of the CVMMT surfaces with CV and/or other pollutants may change with CV surface coverage. These findings are of superlative importance for the design of adsorbents and in understanding the effect of the interacting molecules on the final characteristics of the sorbent/sorbate system.

Acknowledgments

The authors acknowledge Universidad Nacional de San Martín, Ministerio de Ciencia, Tecnología e Innovación Productiva, Agencia Nacional de Promoción Científica y Tecnológica, Fondo para la Investigación Científica y Tecnológica (MINCyT-ANPCyT-FONCyT) for financial support through FONARSEC FS-Nano-08 and PICT 2014-2386 grants. SAXS-WAXS analyses were performed at LNLS, Campinas, Brazil, through project D11A - SAXS1 – 16101. The authors appreciate the support given by LNLS staff. Authors are also thankful to Consejo Nacional de Investigaciones Científicas y Técnicas de la República Argentina (CONICET). M.S.O thanks to DAAD and CONICET for the PVCE fellowship (Program of Scientific Visits Abroad).

Appendix A. Supplementary data

Supplementary data associated with this article can be found, in the online version, at http://dx.doi.org/10.1016/j.cej.2017.09.172.

References

[1] C. Hessel, C. Allegre, M. Maisseu, F. Charbit, P. Moulin, Guidelines and legislation for dye house effluents, J. Environ. Manage. 83 (2007) 171, http://dx.doi.org/10.1016/j.jenvman.2006.02.012.
[2] A. Khalid, S. Mahmood, The biodegradation of azo dyes by actinobacteria, in: S.N. Singh (Ed.), Microbial Degradation of Synthetic Dyes in Wastewaters, Springer International Publishing, 2014, pp. 297–314.
[3] S. Popli, U.D. Patel, Destruction of azo dyes by anaerobic-aerobic sequential biological treatment: a review, Int. J. Environ. Sci. Technol. 12 (2015) 405, http://dx.doi.org/10.1007/s13762-014-0499-x.
[4] J.L. Marco-Brown, M.A. Trinelli, E.M. Gaigneaux, R.M. Torres Sánchez, M. dos Santos Afonso, New insights on the structure of the picloram-montmorillonite surface complexes, J. Colloid Interface Sci. 444 (2015) 115, http://dx.doi.org/10.1016/j.jcis.2014.12.045.
[5] J.L. Marco-Brown, M.M. Areco, R.M. Torres Sánchez, M. dos Santos Afonso, Adsorption of picloram herbicide on montmorillonite: Kinetic and equilibrium studies, Colloids Surf. A 449 (2014) 121, http://dx.doi.org/10.1016/j.colsurfa.2014.02.038.

[6] V.K. Gupta Suhas, Application of low-cost adsorbents for dye removal - a review, J. Environ. Manage. 90 (2009) 2313, http://dx.doi.org/10.1016/j.jenvman.2008.11.017.

[7] G. Crini, Non-conventional low-cost adsorbents for dye removal: a review, Bioresour. Technol. 97 (2006) 1061, http://dx.doi.org/10.1016/j.biortech.2005.05.001.

[8] I. Ali, M. Asim, T.A. Khan, Low cost adsorbents for the removal of organic pollutants from wastewater, J. Environ. Manage. 113 (2012) 170, http://dx.doi.org/10.1016/j.jenvman.2012.08.028.

[9] K.G. Bhattacharyya, S.S. Gupta, Adsorption of a few heavy metals on natural and modified kaolinite and montmorillonite: a review, Adv. Colloid Interface Sci. 140 (2008) 114, http://dx.doi.org/10.1016/j.cis.2007.12.008.

[10] M.S.U. Rehman, M. Munir, M. Ashfaq, N. Rashid, M.F. Nazar, M. Danish, J.-I. Han, Adsorption of Brilliant Green dye from aqueous solution onto red clay, Chem. Eng. J. 228 (2013) 54, http://dx.doi.org/10.1016/j.cej.2013.04.094.

[11] M. Auta, B.H. Hameed, Chitosan–clay composite as highly effective and low-cost adsorbent for batch and fixed-bed adsorption of methylene blue, Chem. Eng. J. 237 (2014) 352, http://dx.doi.org/10.1016/j.cej.2013.09.066.

[12] R. Bhattacharyya, S.K. Ray, Removal of congo red and methyl violet from water using nano clay filled composite hydrogels of poly acrylic acid and polyethylene glycol, Chem. Eng. J. 260 (2015) 269, http://dx.doi.org/10.1016/j.cej.2014.08.030.

[13] M. Rafatullah, O. Sulaiman, R. Hashim, A. Ahmad, Adsorption of methylene blue on low-cost adsorbents: a review, J. Hazard. Mater. 177 (2010) 70, http://dx.doi.org/10.1016/j.jhazmat.2009.12.047.

[14] S.S. Tahir, N. Rauf, Removal of a cationic dye from aqueous solutions by adsorption onto bentonite clay, Chemosphere 63 (2006) 1842, http://dx.doi.org/10.1016/j.chemosphere.2005.10.033.

[15] L. Guz, G. Curutchet, R.M. Torres Sánchez, R. Candal, Adsorption of crystal violet on montmorillonite (or iron modified montmorillonite) followed by degradation through Fenton or photo-Fenton type reactions, J. Environ. Chem. Eng. 2 (2014) 2344, http://dx.doi.org/10.1016/j.jece.2014.02.007.

[16] R. Zhu, Q. Chen, Q. Zhou, Y. Xi, J. Zhu, H. He, Adsorbents based on montmorillonite for contaminant removal from water: a review, Appl. Clay Sci. 123 (2016) 239, http://dx.doi.org/10.1016/j.clay.2015.12.024.

[17] D.J. Alderman, Malachite green: a review, J. Fish Dis. 8 (1985) 289, http://dx.doi.org/10.1111/j.1365-2761.1985.tb00945.x.

[18] S.J. Culp, F.A. Beland, Malachite green: a toxicological review, Int. J. Toxicol. 15 (1996) 219, http://dx.doi.org/10.3109/10915819609008715.

[19] L.L. Schramm, S. Yariv, D.K. Ghosh, L.G. Hepler, Electrokinetic study of the adsorption of ethyl violet and crystal violet by montmorillonite clay particles, Can. J. Chem. 75 (1997) 1868, http://dx.doi.org/10.1139/v97-620.

[20] C. Dobrogowska, L.G. Hepler, D.K. Ghosh, S. Yariv, Metachromasy in clay mineral systems - Spectrophotometric and calorimetric study of the adsorption of crystal-violet and ethyl violet by Na-montmorillonit and by Na-kaolinite, J. Therm. Anal. 37 (1991) 1347, http://dx.doi.org/10.1007/BF01913866.

[21] S. Yariv, M. Müller-Vonmoos, G. Kahr, A. Rub, Thermal analytic study of the adsorption of crystal violet by montmorillonite, Thermochim. Acta 148 (1989) 457, http://dx.doi.org/10.1016/0040-6031(89)85247-5.

[22] L.G. Hepler, S. Yariv, C. Dobrogowska, Calorimetric investigation of adsorption of an aqueous metachromic dye (crystal-violet) on montmorillonite, Thermochim. Acta 121 (1987) 373, http://dx.doi.org/10.1016/0040-6031(87)80187-9.

[23] S. Yariv, D.K. Ghosh, L.G. Hepler, Metachromasy in clay-mineral systems: adsorption of cationic dyes crystal violet and ethyl violet by kaolinite from aqueous and organic solutions, J. Chem. Soc. Faraday Trans. 87 (1991) 1201, http://dx.doi.org/10.1039/FT9918701201.

[24] P. Pustková, Z. Klika, J. Preclikova, T.M. Grygar, Enhanced fluorescence of selected cationic dyes adsorbed on reduced-charge montmorillonite, Clay Miner. 46 (2011) 93, http://dx.doi.org/10.1180/claymin.2011.046.1.93.

[25] I. Lapides, S. Yariv, D. Golodnitsky, Simultaneous DTA-TG study of montmorillonite mechanochemically treated with crystal-violet, J. Therm. Anal. Calorim. 67 (2002) 99, http://dx.doi.org/10.1023/A:1013737914178.

[26] Z. Chernia, D. Gill, S. Yariv, Electric dichroism. The effect of dialysis on the color of crystal violet adsorbed to montmorillonite, Langmuir 10 (1994) 3988, http://dx.doi.org/10.1021/la00023a015.

[27] G.K. Sarma, S. Sen Gupta, K.G. Bhattacharyya, Adsorption of Crystal violet on raw and acid-treated montmorillonite, K10, in aqueous suspension, J. Environ. Manage. 171 (2016) 1, http://dx.doi.org/10.1016/j.jenvman.2016.01.038.

[28] R. Zhu, Q. Chen, H. Liu, F. Ge, L. Zhu, J. Zhu, H. He, Montmorillonite as a multifunctional adsorbent can simultaneously remove crystal violet, cetyltrimethylammonium, and 2-naphthol from water, Appl. Clay Sci. 88–89 (2014) 33, http://dx.doi.org/10.1016/j.clay.2013.12.010.

[29] J. Wei, R. Zhu, J. Zhu, F. Ge, P. Yuan, H. He, C. Ming, Simultaneous sorption of crystal violet and 2-naphthol to bentonite with different CECs, J. Hazard. Mater. 166 (2009) 195, http://dx.doi.org/10.1016/j.jhazmat.2008.11.004.

[30] Q. Chen, H. Liu, R. Zhu, X. Wang, S. Wang, J. Zhu, H. He, Facile synthesis of nitrogen and sulfur co-doped graphene-like carbon materials using methyl blue/montmorillonite composites, Micropor. Mesopor. Mater. 225 (2016) 137, http://dx.doi.org/10.1016/j.micromeso.2015.12.026.

[31] R. Zhu, Q. Chen, X. Wang, S. Wang, J. Zhu, H. He, Templated synthesis of nitrogen-doped graphene-like carbon materials using spent montmorillonite, RSC Adv. 5 (2015) 7522, http://dx.doi.org/10.1039/C4RA13732A.

[32] X.S. Wang, W. Zhang, Removal of basic dye crystal violet from aqueous solution by Cu(II)-loaded montmorillonite, Sep. Sci. Technol. 46 (2011) 656, http://dx.doi.org/10.1080/01496395.2010.517823.

[33] F. Geyikçi, The equilibrium and kinetics studies of crystal violet adsorption onto montmorillonite, Environ. Eng. Manage. J. 11 (2012) 733.

[34] A. Czímerová, J. Bujdák, R. Dohrmann, Traditional and novel methods for estimating the layer charge of smectites, Appl. Clay Sci. 34 (2006) 2, http://dx.doi.org/10.1016/j.clay.2006.02.008.

[35] M. Tschapek, R.M.T. Sanchez, C. Wasowski, Handy methods for determining the isoelectric point of soils, Zeitschrift für Pflanzenernährung und Bodenkunde 152 (1989) 73, http://dx.doi.org/10.1002/jpln.19891520113.

[36] A.P. Magnoli, L. Tallone, C.A.R. Rosa, A.M. Dalcero, S.M. Chiacchiera, R.M. Torres Sanchez, Commercial bentonites as detoxifier of broiler feed contaminated with aflatoxin, Appl. Clay Sci. 40 (2008) 63, http://dx.doi.org/10.1016/j.clay.2007.07.007.

[37] D. Siguín, S. Ferreira, L. Froufe, F. García, Smectites: the relationship between their properties and isomorphic substitution, J. Mater. Sci. 29 (1994) 4379, http://dx.doi.org/10.1007/BF00414225.

[38] M. Gamba, F.M. Flores, J. Madejová, R.M. Torres Sánchez, Comparison of imazalil removal onto montmorillonite and nanomontmorillonite and adsorption surface sites involved: an approach for agricultural wastewater treatment, Ind. Eng. Chem. Res. 54 (2015) 1529, http://dx.doi.org/10.1021/ie5035804.

[39] B. Schampera, S. Dultz, The effect of surface charge and wettability on H_2O self diffusion in compacted clays, Clay. Clay Miner. 59 (2011) 42, http://dx.doi.org/10.1346/CCMN.2011.0590107.

[40] B. Schampera, S. Dultz, Determination of diffusive transport in HDPy-montmorillonite by H_2O–D_2O exchange using in situ ATR-FTIR spectroscopy, Clay Miner. 44 (2009) 249, http://dx.doi.org/10.1180/claymin.2009.044.2.249.

[41] J.H. An, S. Dultz, Adsorption of tannic acid on chitosan-montmorillonite as a function of pH and surface charge properties, Appl. Clay Sci. 36 (2007) 256, http://dx.doi.org/10.1016/j.clay.2006.11.001.

[42] B. Schampera, D. Tunega, R. Šolc, S.K. Woche, R. Mikutta, R. Wirth, S. Dultz, G. Guggenberger, External surface structure of organoclays analyzed by transmission electron microscopy and X-ray photoelectron spectroscopy in combination with molecular dynamics simulations, J. Colloid Interface Sci. 478 (2016) 188, http://dx.doi.org/10.1016/j.jcis.2016.06.008.

[43] B. Schampera, R. Šolc, D. Tunega, S. Dultz, Experimental and molecular dynamics study on anion diffusion in organically modified bentonite, Appl. Clay Sci. 120 (2016) 91, http://dx.doi.org/10.1016/j.clay.2015.11.026.

[44] B. Schampera, R. Solc, S.K. Woche, R. Mikutta, S. Dultz, G. Guggenberger, D. Tunega, Surface structure of organoclays as examined by X-ray photoelectron spectroscopy and molecular dynamics simulations, Clay Miner. 50 (2015) 353, http://dx.doi.org/10.1180/claymin.2015.050.3.08.

[45] J. Cheriaa, M. Khaireddine, M. Rouabhia, A. Bakhrouf, Removal of triphenylmethane dyes by bacterial consortium, Sci. World J. 2012 (2012), http://dx.doi.org/10.1100/2012/512454.

[46] Q. Chen, R. Zhu, W. Deng, Y. Xu, J. Zhu, Q. Tao, H. He, From used montmorillonite to carbon monolayer–montmorillonite nanocomposites, Appl. Clay Sci. 100 (2014) 112, http://dx.doi.org/10.1016/j.clay.2014.04.011.

[47] X.-f. Tan, Y.-g. Liu, Y.-l. Gu, S.-b. Liu, G.-m. Zeng, X. Cai, X.-j. Hu, H. Wang, S.-m. Liu, L.-h. Jiang, Biochar pyrolyzed from MgAl-layered double hydroxides pre-coated ramie biomass (Boehmeria nivea (L.) Gaud.): characterization and application for crystal violet removal. J. Environ. Manage. 184, Part 1 (2016) 85. http://dx.doi.org/10.1016/j.jenvman.2016.08.070.

[48] M. Singh, H.S. Dosanjh, H. Singh, Surface modified spinel cobalt ferrite nanoparticles for cationic dye removal: kinetics and thermodynamics studies, J. Water Process Eng. 11 (2016) 152, http://dx.doi.org/10.1016/j.jwpe.2016.05.006.

[49] P.Z. Araujo, P.J. Morando, E. Martínez, M.A. Blesa, Time evolution of surface speciation during heterogeneous photocatalysis: gallic acid on titanium dioxide, Appl. Catal. B 125 (2012) 215, http://dx.doi.org/10.1016/j.apcatb.2012.05.035.

[50] P.Z. Araujo, P.J. Morando, M.A. Blesa, Interaction of catechol and gallic acid with titanium dioxide in aqueous suspensions. 1. Equilibrium studies, Langmuir 21 (2005) 3470, http://dx.doi.org/10.1021/la0476985.

[51] J.L. Marco-Brown, M.A. Blesa, G.J.A.A. Soler-Illia, Preparation of mesoporous titania xerogels under controlled synthesis conditions Effects of processing in the textural, adsorption and photocatalytic properties, Colloids Surf. A Physicochem. Eng. Aspects 530 (2017) 93, http://dx.doi.org/10.1016/j.colsurfa.2017.07.054.

[52] P.Z. Araujo, V. Luca, P.B. Bozzano, H.L. Bianchi, G.J.A.A. Soler-Illia, M.A. Blesa, Aerosol-assisted production of mesoporous titania microspheres with enhanced photocatalytic activity: the basis of an improved process, ACS Appl. Mater. Interf. 2 (2010) 1663, http://dx.doi.org/10.1021/am100188q.

[53] M. Haerifar, S. Azizian, Mixed surface reaction and diffusion-controlled kinetic model for adsorption at the solid/solution interface, J. Phys. Chem. C 117 (2013) 8310, http://dx.doi.org/10.1021/jp401571m.

[54] M.M. Areco, L. Saleh-Medina, M.A. Trinelli, J.L. Marco-Brown, M. dos Santos Afonso, Adsorption of Cu(II), Zn(II), Cd(II) and Pb(II) by dead Avena fatua biomass and the effect of these metals on their growth, Colloids Surf. B 110 (2013) 305, http://dx.doi.org/10.1016/j.colsurfb.2013.04.035.

[55] A.K. Bhattacharya, C. Venkobachar, Removal of Cadmium (II) by low cost adsorbents, J. Environ. Eng. 110 (1984) 110, http://dx.doi.org/10.1061/(ASCE)0733-9372(1984)110:1(110).

[56] R.R. Pawar, P. Gupta, H.C. Lalhmunsiama, S.-M. Lee Bajaj, Al-intercalated acid activated bentonite beads for the removal of aqueous phosphate, Sci. Total Environ. 572 (2016) 1222, http://dx.doi.org/10.1016/j.scitotenv.2016.08.040.

[57] W.J. Weber, J.C. Morris, Kinetics of adsorption carbon from solutions, J. Sanitary Eng. Div. Proc. Am. Soc. Civ. Eng. 89 (1963) 31.

[58] X. Peng, F. Hu, J. Huang, Y. Wang, H. Dai, Z. Liu, Preparation of a graphitic ordered mesoporous carbon and its application in sorption of ciprofloxacin: Kinetics, isotherm, adsorption mechanisms studies, Micropor. Mesopor. Mater. 228 (2016) 196, http://dx.doi.org/10.1016/j.micromeso.2016.03.047.

[59] Q. Sun, L. Yang, The adsorption of basic dyes from aqueous solution on modified peat–resin particle, Water Res. 37 (2003) 1535, http://dx.doi.org/10.1016/S0043-1354(02)00520-1.
[60] M. Doğan, H. Abak, M. Alkan, Adsorption of methylene blue onto hazelnut shell: kinetics, mechanism and activation parameters, J. Hazard. Mater. 164 (2009) 172, http://dx.doi.org/10.1016/j.jhazmat.2008.07.155.
[61] J.Z. Guo, B. Li, L. Liu, K. Lv, Removal of methylene blue from aqueous solutions by chemically modified bamboo, Chemosphere 111 (2014) 225, http://dx.doi.org/10.1016/j.chemosphere.2014.03.118.
[62] G.E. Boyd, A.W. Adamson, L.S. Myers Jr, The exchange adsorption of ions from aqueous solutions by organic zeolites. II. Kinetics, J. Am. Chem. Soc. 69 (1947) 2836, http://dx.doi.org/10.1021/ja01203a066.
[63] HyperChem(TM) Professional 8.05, Hypercube-Inc., 1115 NW 4th Street, Gainesville, Florida 32601, USA.
[64] A. Kiersnowski, M. Trelińska-Wlaźlak, M. Gazińska, J. Pigłowski, X-ray scattering and calorimetric studies of organoclays obtained by ion-exchange, Polim 56 (2011) 671.
[65] A.E. Bianchi, M. Fernández, M. Pantanetti, R. Viña, I. Torriani, R.M. Torres Sánchez, G. Punte, $ODTMA^+$ and $HDTMA^+$ organo-montmorillonites characterization: new insight by WAXS, SAXS and surface charge, Appl. Clay Sci. 83–84 (2013) 280, http://dx.doi.org/10.1016/j.clay.2013.08.032.
[66] J. Rouquerol, F. Rouquerol, K.S.W. Sing, Chapter 11-Adsorption by Clays, Pillared Layer Structures and Zeolites, Adsorption by Powders and Porous Solids. Principles, Methodology and Applications; Academic Press, 24–28 Oval Road, London NW1 7DX, UK, 1999, pp. 355–399.